



Published in final edited form as:

*Nanomedicine*. 2020 April ; 25: 102169. doi:10.1016/j.nano.2020.102169.

## Induction of Antitumor Immunity in Mice by the Combination of Nanoparticle-Based Photothermolysis and Anti-PD-1 Checkpoint Inhibition

Qizhen Cao, Ph.D.<sup>1</sup>, Wanqin Wang, M.D.<sup>1,2</sup>, Min Zhou, Ph.D.<sup>1,3</sup>, Qian Huang, M.D.<sup>1</sup>, Xiaoxia Wen, M.S.<sup>1</sup>, Jun Zhao, Ph.D.<sup>1</sup>, Sixiang Shi, Ph.D.<sup>1</sup>, Ku Geng, Ph.D.<sup>1</sup>, Fenge Li, M.D.<sup>4</sup>, Hiroto Hatakeyama, Ph.D.<sup>5</sup>, Chunyu Xu, M.S.<sup>4</sup>, David Piwnica-Worms, Ph.D.<sup>1</sup>, Weiyi Peng, Ph.D.<sup>4</sup>, Dapeng Zhou, Ph.D.<sup>4,6</sup>, Anil K. Sood, M.D.<sup>5</sup>, Chun Li, Ph.D.<sup>1,\*</sup>

<sup>1</sup>Department of Cancer Systems Imaging, The University of Texas MD Anderson Cancer Center, 1881 East Road, Houston, TX 77054, USA

<sup>2</sup>Current Address: Department of Radiology, The 1st Affiliated Hospital of Anhui Medical University, Hefei, Anhui, China

<sup>3</sup>Current Address: The Second Affiliated Hospital, Institute of Translational Medicine, Zhejiang University School of Medicine, 310029, China

<sup>4</sup>Department of Melanoma Medical Oncology, The University of Texas MD Anderson Cancer Center, 1881 East Road, Houston, TX 77054, USA

<sup>5</sup>Departments of Gynecologic Oncology & Reproductive Medicine and Cancer Biology, The University of Texas MD Anderson Cancer Center, 1881 East Road, Houston, TX 77054, USA

<sup>6</sup>Current Address: Shanghai Pulmonary Hospital, Tongji University School of Medicine, Shanghai, 200092, China

### Abstract

Generation of durable tumor-specific immune response without isolation and expansion of dendritic cells or T cells *ex vivo* remains a challenge. In this study, we investigated the impact of nanoparticle-mediated photothermolysis in combination with checkpoint inhibition on the induction of systemic antitumor immunity. Photothermolysis based on near-infrared light-absorbing copper sulfide nanoparticles and 15-ns laser pulses combined with the immune checkpoint inhibitor anti-PD-1 antibody ( $\alpha$ PD-1) increased tumor infiltration by antigen-presenting cells and CD8-positive T lymphocytes in the B16-OVA mouse model. Moreover, combined photothermolysis, polymeric conjugate of the Toll-like receptor 9 agonist CpG, and  $\alpha$ PD-1 significantly prolonged mouse survival after re-inoculation of tumor cells at a distant site compared to individual treatments alone in the poorly immunogenic syngeneic ID8-ip1-Luc

\* **Corresponding Author:** Chun Li, PhD, Department of Cancer Systems Imaging, 1881 East Road–Unit 1907, The University of Texas MD Anderson Cancer Center, Houston, Texas 77054; Tel: 713-792-5182; Fax: 713-794-5456; cli@mdanderson.org.

**Publisher's Disclaimer:** This is a PDF file of an unedited manuscript that has been accepted for publication. As a service to our customers we are providing this early version of the manuscript. The manuscript will undergo copyediting, typesetting, and review of the resulting proof before it is published in its final form. Please note that during the production process errors may be discovered which could affect the content, and all legal disclaimers that apply to the journal pertain.

**Competing Interests:** The authors have declared that no competing interest exists.

ovarian tumor model. Thus, photothermolysis is a promising interventional technique that synergizes with Toll-like receptor 9 agonists and immune checkpoint inhibitors to enhance the abscopal effect in tumors.

## Graphical Abstract

In a poorly immunogenic syngeneic ovarian cancer model, short-pulsed wave (PW) laser photothermolysis based on near-infrared light-absorbing copper sulfide nanoparticles, combined with polymeric conjugate of the Toll-like receptor 9 agonist CpG and the immune checkpoint inhibitor anti-PD-1 antibody, significantly induced systemic immune response and prolonged mouse survival after re-inoculation of tumor cells at a distant site, compared to individual treatments alone.

## Keywords

CuS nanoparticle; Pulsed laser; Photothermolysis; Abscopal effect; Checkpoint inhibitor

---

## Introduction

Copper chalcogenide nanoparticles (NPs) exhibit strong absorption in the near-infrared (NIR) region, demonstrate highly efficient light-to-heat transformation under NIR laser irradiation, and cause selective thermal destruction of tumor.<sup>1–4</sup> Given that copper monosulfide (CuS) NPs can be synthesized using a remarkably simple process at low cost, CuS NPs have emerged as a new class of photothermal conducting agents.

Thermal therapy is a promising minimally-invasive technique currently being investigated for the treatment of a variety of solid tumors.<sup>5</sup> One thermal therapy currently under investigation is laser-induced thermal therapy mediated by multifunctional NPs.<sup>3, 6</sup> A commonly used laser system for NP-mediated laser-induced thermal therapy is continuous-wave laser, which kills cells by coagulative necrosis at high temperature (>50 °C).<sup>7</sup> Another form of thermal therapy is irradiation of tumor cells with short pulses from pulsed-wave (PW) laser in the presence of NIR light-absorbing NPs, which kills cells by producing a combined photothermal and photomechanical effect (hereafter referred to as photothermolysis).<sup>8, 9</sup> One of the advantages of photothermolysis with PW laser over photothermal ablation with continuous-wave laser is excellent spatial and temporal control in mediating cell death.<sup>10</sup> Another advantage is that under similar conditions (i.e., power density, interaction time, and beam diameter), PW laser has a much higher penetration depth than continuous-wave laser.<sup>11</sup>

The abscopal effect is a phenomenon by which localized treatment of a tumor causes shrinkage of tumors outside the volume of localized tumor ablation. Most studies about the abscopal effect have focused on radiation therapy,<sup>12–14</sup> radiation therapy has been shown to increase antigen presentation by antigen-presenting cells within the tumor and thereby enhance the killing of tumor cells by T cells.<sup>15</sup> However, other types of localized treatment are also capable of inducing an abscopal effect, including local oncolytic virotherapy, thermal therapy, and cryoablation.<sup>16–18</sup>

The adaptive immune response plays a key role in induction of the abscopal effect, which requires effective presentation of tumor-associated antigens and T cell co-stimulation.<sup>19</sup> In this process, dying tumor cells expel intracellular tumor-specific antigens previously invisible to the immune system. These antigens are subsequently processed by antigen-presenting cells, of which dendritic cells (DCs) are the most important. Antigen-loaded DCs then migrate to the regional lymph nodes, where they present the processed antigens to T cells.<sup>20</sup> For DCs to activate T cells, DCs themselves must be activated by “danger signals” from exposure to damage-associated molecular patterns such as heat-shock proteins and Toll-like receptor ligands.<sup>7,21</sup> Toll-like receptor 9 agonist CpG mimics microbial DNA and elicits a coordinated set of immune responses, including activation of innate immune cells and activation of specific T cells (adaptive immunity).<sup>21,22</sup> We have used a biocompatible, biodegradable polymer, poly(L-glutamic acid) (PG), to direct and control the release of CpG at tumor sites. We previously showed that CpG chemically bound to PG (PG-CpG) was retained significantly longer in both tumor and draining lymph nodes than free CpG after intratumoral injection and displayed strong antitumor effects.<sup>23</sup>

The intensity of the immune response is determined by the balance between costimulatory signals and inhibitory immune checkpoints.<sup>24</sup> Targeting immune checkpoints such as programmed death 1 (PD-1), programmed death 1 ligand 1, and cytotoxic T-lymphocyte antigen-4 has demonstrated significant clinical activity in melanoma and lung cancer, but not yet in many other solid tumors.<sup>25–27</sup> In light of the remarkable results with checkpoint inhibitors, a major question in the field is how to broaden these responses to more tumor types, including those with a relatively low mutational load, such as ovarian cancer. It is believed that T cell recognition of tumor-specific antigens contributes to the efficacy of checkpoint inhibitors and that tumors with a higher mutational burden are more likely to generate an antitumor adaptive immune response.<sup>28</sup> In ovarian cancer, tumors with higher mutational load exhibit more tumor-infiltrating lymphocytes and are associated with better overall survival.<sup>29</sup>

In the current work, we investigated the effect of photothermolysis based on CuS NPs in the presence and absence of immune checkpoint inhibitor anti-PD-1 antibody ( $\alpha$ PD-1) in the 1316-OVA murine melanoma model. Moreover, we used a poorly immunogenic syngeneic ovarian cancer model to assess the effect of combined photothermolysis, PG-CpG, and  $\alpha$ PD-1 in delaying distant tumor growth after tumor cell challenge. Our data showed that such therapy produced durable responses with memory T cells in a fraction of treated mice.

## Methods

### Materials

Copper(II) chloride ( $\text{CuCl}_2$ ), sodium sulfide ( $\text{Na}_2\text{S}\cdot 9\text{H}_2\text{O}$ ), PG, and methoxy-PEG-thiol (PEG-SH, molecular weight 5000) were purchased from Sigma-Aldrich (St. Louis, MO, USA). CpG oligonucleotide (ODC 2216) with 3' terminal-amino group (5'-EEGGGACGATCGTCEEEEG-3-NH<sub>2</sub>, CpG-3'-NH<sub>2</sub>) was purchased from Invitrogen (Chicago, IL, USA). Monoclonal anti-mouse PD-1 (CD279, clone: J43) was purchased from Bio X Cell (West Lebanon, NH, USA).

### General procedure for the synthesis of PEGylated CuS NPs (PEG-CuS NPs)

For the synthesis of PEG-CuS NPs, 0.1 mL of sodium sulfide solution ( $\text{Na}_2\text{S}$ , 1 M) was added into 100 mL of an aqueous solution of  $\text{CuCl}_2$  (0.1 mmol) and PEG-SH (0.2 mmol) under stirring at room temperature. Starting 5 min later, the reaction mixture was heated to 90 °C and stirred at 1000 rpm for 15 min until a dark green solution was obtained. NPs with peak absorption at 990 nm were obtained by adjusting the stoichiometric ratio between  $\text{CuCl}_2$  and  $\text{Na}_2\text{S}$ . Free  $\text{CuCl}_2$ , PEG-SH, and  $\text{Na}_2\text{S}$  were removed by an ultra-centrifugal filter unit (Amicon Ultra-15, 50 kDa, Billerica, MA, USA).

### Characterization of CuS NPs

The ultraviolet–visible absorption spectra of PEG-CuS NPs were measured on a UV–Vis spectrometer (DU-800, Beckman Coulter, Atlanta, GA). Particle size was characterized by using a dynamic light scattering instrument (Brookhaven Instruments, Holtsville, NY) and by transmission electron microscopy using a JEM 1010 transmission electron microscope (JEOL USA, Inc., Peabody, MA).

### Synthesis of radioactive PEG-[ $^{64}\text{Cu}$ ]CuS NPs and $^{64}\text{Cu}$ -labeled $\alpha\text{CD11b}$

Chelator-free radioactive PEG-[ $^{64}\text{Cu}$ ]CuS NPs were synthesized according to reported procedures.<sup>4</sup> Briefly,  $^{64}\text{CuCl}_2$  (20  $\mu\text{L}$ , 1000  $\mu\text{Ci}$ ) was added to 1 mL of  $\text{CuCl}_2$  solution (1 mM) containing 1 mg PEG-SH. Then, 10  $\mu\text{L}$  of sodium sulfide solution (100 mM) was added to the  $\text{CuCl}_2$  solution under stirring. The mixture was then heated to 90 °C for 15 min. The reaction mixture was transferred to ice-cold water to give PEG-[ $^{64}\text{Cu}$ ]CuS NPs.

$^{64}\text{Cu}$ -labeled  $\alpha\text{CD11b}$  was synthesized according to reported procedures.<sup>30</sup>

### Synthesis of PG-CpG

PG-CpG was synthesized and characterized as previously described.<sup>23</sup>

### Laser systems

A 1064-nm Q-switched Nd:YAG PW laser system at a repetition rate of 10 Hz with a 15-ns pulse width (Lotis Tii; Symphotic, Minsk, Belarus) was used in this study. The incident laser energy density of the sample was measured by using a pyroelectric energy meter (PE25-C, Ophir, North Logan, UT). The laser energy fluence was calculated according to an established calibration curve.

To determine the impact of combined photothermolysis and  $\alpha\text{PD-1}$  immunotherapy in the B16-OVA tumor model, PW laser at a power density of 2.2  $\text{W}/\text{cm}^2$  for 45 s was used.

To determine the impact of combined photothermolysis, PG-CpG, and  $\alpha\text{PD-1}$  immunotherapy in the ID8-ip1-Luc ovarian cancer model, PW laser at a power density of 2.2  $\text{W}/\text{cm}^2$  for 1 or 2 min was used.

### Animal models and tumor cell lines

All animal experiments were performed in compliance with the guidelines for care and use of research animals established by the Institutional Animal Care and Use Committee of The

University of Texas MD Anderson Cancer Center (Protocol #00000736). Female C57BL/6 mice (6-8 weeks of age) were obtained from Taconic (Cambridge City, IN). B16-OVA (B16F10 cells expressing ovalbumin) and ID8-ip1-Luc cell lines were confirmed with short tandem repeat DNA fingerprinting method by IDEXX BioResearch when the cells were used in this study.

### Biodistribution

C57BL/6 mice were inoculated with B16F10 cells ( $5 \times 10^5$  cells/mouse) or ID8-ip1-Luc cells ( $5 \times 10^6$  cells/mouse) subcutaneously. When tumors had reached an average three-dimensional size of 6 mm, mice received an intravenous injection of PEG- $^{64}\text{Cu}$ CuS (~60  $\mu\text{Ci}$ , 0.2 mL per mouse). Mice were euthanized at 24 h post-injection. Blood, major organs, and tumor tissues were collected, wet-weighed, and counted in a  $\gamma$ -counter (Packard, Waltham, MA, USA). The results were normalized to 25 g mouse body weight and reported as the mean of percentage injected dose per gram (%ID/g)  $\pm$  standard deviation (n = 5).

### $\mu\text{PET/CT}$ imaging

$\mu\text{PET/CT}$  was performed using an Inveon scanner (Siemens Medical Solutions, Erlangen, Germany). Each mouse was anesthetized and injected with 200  $\mu\text{Ci}$  of PEG- $^{64}\text{Cu}$ CuS or  $^{64}\text{Cu}$ -labeled  $\alpha\text{CD11b}$  intravenously via tail vein, and images were acquired at 24 h post-injection. Imaging data were analyzed using Inveon software (Siemens) and expressed as % ID/g.

### Impact of photothermalolysis with PEG-CuS NPs and PW laser on B16-OVA melanoma cells in vitro

B16-OVA melanoma cells were seeded in 48-well plates ( $5 \times 10^4$  cells/well) for 24 h. Cells were then incubated with PEG-CuS NPs (2 OD, 100  $\mu\text{g/mL}$ ) for 2 h, washed with PBS, and irradiated with PW laser (2.2  $\text{W/cm}^2$  for 2 min). Cells were photographed at 24 h and 48 h after laser treatment and then stained with trypan blue and photographed at 48 h.

### Impact of combined photothermalolysis and $\alpha\text{PD-1}$ on B 16-OVA tumor-bearing mice

Mice with subcutaneously inoculated B16-OVA tumors ( $3 \times 10^5$  cells/site) were randomly divided into four groups when tumors reached around 6 mm in mean diameter ( $\sim 100 \text{ mm}^3$ ): 1) untreated control, 2)  $\alpha\text{PD-1}$  only, 3) photothermalolysis (PEG-CuS NPs with PW laser) only, and 4) photothermalolysis (PEG-CuS NPs with PW laser) plus  $\alpha\text{PD-1}$ . Mice in groups 3 and 4 were injected intravenously with PEG-CuS NPs (8 OD [1 OD = 50  $\mu\text{g/mL}$ ], 200  $\mu\text{L}$ /mouse) on day 0, and B16-OVA tumors were treated with PW laser at 1064 nm (2.2  $\text{W/cm}^2$ , 45 s) on day 1. Mice in groups 2 and 4 were intraperitoneally injected with  $\alpha\text{PD-1}$  (100  $\mu\text{g}/100 \mu\text{L}$ /mouse) on days 2, 4, and 6. Tumor growth was monitored as described above. B16-OVA tumors were collected on days 7-9 and analyzed for infiltrated immune cells.

### Impact of combined photothermalolysis, PG-CpG, and $\alpha\text{PD-1}$ on ID8-ip1-Luc ovarian cancer bearing mice

**First independent experiment:** Mice were subcutaneously inoculated with ID8-ip1-Luc cells ( $3 \times 10^6$  cells). When tumors reached around 6 mm in diameter, mice were randomly

divided into four groups: 1) untreated control; 2) PG-CpG plus  $\alpha$ -PD-1; 3) photothermolysis (PEG-CuS NPs with PW laser); and 4) photothermolysis (PEG-CuS NPs with PW laser) plus PG-CpG plus  $\alpha$ -PD-1. Mice in groups 3 and 4 were injected intravenously with PEG-CuS NPs (8 OD, 400  $\mu$ g/mL, 200  $\mu$ L/mouse) on day 0, and ID8-ip1-Luc tumors were treated with pulsed laser (2.2 W/cm<sup>2</sup>, 1 min) on day 1. Mice in groups 3 and 4 received an intratumoral injection of the second dose of PEG-CuS NPs (8 OD, 400  $\mu$ g/mL, 20  $\mu$ L/mouse) on day 7, and ID8-ip1-Luc tumors were treated with pulsed laser (2.2 W/cm<sup>2</sup>, 1 min) on day 8. Mice in groups 2 and 4 were injected intratumorally with PG-CpG (50  $\mu$ g/mouse) after the second laser treatment. All mice were challenged with an intraperitoneal injection of ID8-ip1-Luc cells ( $1 \times 10^6$  cells) on day 9. On days 9, 12, and 15, mice in groups 2 and 4 were injected intraperitoneally with  $\alpha$ -PD-1 (200  $\mu$ g/200  $\mu$ L/mouse). Mouse body weight was measured once every three days.

**Second independent experiment:** This experiment was designed to compare the antitumor effect of one versus two rounds of photothermolysis. Mice were subcutaneously inoculated with ID8-ip1-Luc cells ( $3 \times 10^6$  cells/site). When tumors reached around 6 mm in diameter, mice were randomly divided into five groups: 1) untreated control; 2) one dose of PEG-CuS NPs with laser treatment; 3) one dose of PEG-CuS NPs with laser treatment plus PG-CpG plus  $\alpha$ -PD-1; 4) two doses of PEG-CuS NPs with laser treatments; and 5) two doses of PEG-CuS NPs with laser treatments plus PG-CpG and  $\alpha$ -PD-1. Mice in groups 2 and 3 received a single intravenous injection of PEG-CuS NPs (20 OD, 1 mg/mL, 200  $\mu$ L/mouse) and were treated with PW laser (2.2 W/cm<sup>2</sup>, 2 min) once. Mice in groups 4 and 5 received two intravenous injections of PEG-CuS NPs (20 OD, 1 mg/mL, 200  $\mu$ L/mouse) and were treated with PW laser (2.2 W/cm<sup>2</sup>, 2 min) twice, each time 1 day after each PEG-CuS NP injection. Mice in groups 3 and 5 were injected intratumorally with PG-CpG (50  $\mu$ g/mouse) after laser treatment. All mice were challenged with a second intraperitoneal injection of ID8-ip1-Luc cells ( $1 \times 10^6$  cells) on day 10. On days 9, 12, and 15, mice in groups 3 and 5 were injected intraperitoneally with  $\alpha$ -PD-1 (200  $\mu$ g/200  $\mu$ L/mouse). Mouse body weight was measured once every three days.

### Analyses of immune cell infiltration into B16-OVA tumors with flow cytometry

B16-OVA tumor tissues were collected 1 week after laser treatment. Single-cell suspensions were prepared by mincing tumor tissue with scissors and then filtering it through a Falcon 70- $\mu$ m nylon filter (Thermo Fisher Scientific, Asheville, NC, USA). Cells were washed with PBS and blocked with PBS 1% BSA. Subsequently, cells were incubated for 1 hour with one or more of the following antibodies (Thermo Fisher): PE-eFluor610 anti-CD45, PerCP/Cy5.5-CD3, APC-eFluor780 anti-CD8, eFluor450-CD4, APC-CD25, PE-FoxP3, eFluor450-CD45, PE-CD11b, PerCP/Cy5.5-Gr-1, eFluor660-CD169, or Alexa Fluor700-CD11c. Aqua (Invitrogen) was used to discriminate between live and dead cells. Cells were then washed twice with PBS containing 1% BSA. Samples were run on an LSRFortessa X-20 analyzer (BD Biosciences) and analyzed using FlowJo software (Tree Star Inc.).

### Memory T cell detection in spleens of long-term-surviving mice

Spleens were collected from the long-term-surviving mice and dissociated into single splenocytes. After red blood cell lysis, splenocytes were incubated with rat anti-mouse

CD16/CD32 Fcγ III/II receptor for 30 min at 4 °C to block Fc receptors. Subsequently, cells were incubated with fluorescence probes (Thermo Fisher) for 30 min on ice. These fluorescence probes included PerCP/Cy5.5-CD4, PE/Cy7-CD8, Pacific Blue-CD62L, and FITC-CD44. Cells were then washed twice with PBS, and cell samples were run on an LSRFortessa X-20 analyzer and analyzed using FlowJo software.

### ELI SPOT assay

Lysate of tumor cells was prepared by freeze-then-thaw. Mouse DCs were generated from bone marrow mononuclear cells by culturing for 7 days in the presence of granulocyte-macrophage colony-stimulating factor.<sup>31</sup> DCs were pulsed with tumor lysate for 3 hours at 37 °C and then co-incubated with splenocytes overnight at 37 °C. The formed interferon-γ (IFN-γ) spots were imaged and counted.

### Statistical analysis

Statistical significance was analyzed by one-way analysis of variance or Student's t-test. P values < 0.05 were considered statistically significant.

## Results

### Synthesis and characterization of PEGylated CuS NPs (PEG-CuS NPs)

The absorption spectrum of the PEG-CuS NPs in aqueous solution peaked at around 990 nm (Supplementary Figure S1A). The mean hydrodynamic diameter of the PEG-CuS NPs was 25.6 nm measured by dynamic light scattering (Supplementary Figure S1B). A transmission electron microscopy photograph of the PEG-CuS NPs is shown in Supplementary Figure S1C; the mean diameter of PEG-CuS NPs measured in the dry state was  $8.9 \pm 3.0$  nm. When PEG-CuS NPs of different concentrations (8 OD or 20 OD) were intratumorally injected into ID8-ip1-Luc tumors, irradiation of the tumors with PW laser elevated tumor temperature in a dose-dependent manner, whereas when no NPs were injected, no change in tumor temperature was observed with laser irradiation (Supplementary Figure S2). This demonstrated that PW laser-induced photothermalolysis was based on near-infrared light-absorbing PEG-CuS NPs.

### Biodistribution of PEG-[<sup>64</sup>Cu]CuS NPs in mice with B16F10 and mice with ID8-ip1-Luc tumors

At 24 h after intravenous injection, the uptakes of PEG-[<sup>64</sup>Cu]CuS NPs in the B16F10 tumor and the ID8-ip1-Luc tumor were  $6.5 \pm 2.58$  %ID/g and  $5.3 \pm 1.35$  %ID/g, respectively (Figure 1). Tumor uptake of PEG-[<sup>64</sup>Cu]CuS NPs in the ID8-ip1-Luc tumors was also confirmed by μPET/CT imaging (Supplementary Figure S3). The NPs had relatively high uptakes in the liver ( $26.3 \pm 3.01$  %ID/g and  $19.7 \pm 3.7$  %ID/g, respectively) and the spleen ( $10.2 \pm 2.9$  %ID/g and  $9.8 \pm 1.0$  %ID/g, respectively) in mice bearing B16F10 or ID8-ip1-Luc tumors (Figure 1). We previously reported that PEG-CuS NPs were biodegradable and had no evident adverse effects on liver function and histopathology in mice.<sup>32–34</sup>

### Combined photothermolysis and $\alpha$ PD-1 increased tumor infiltration of T cells and DCs

To assess the effect of PEG-CuS NP-mediated photothermolysis on tumor cells, B16-OVA cells were incubated with PEG-CuS NPs and then irradiated with PW laser. While no apparent change in cell viability was observed when cells were treated with PEG-CuS NPs alone or PW laser alone, photothermolysis with PEG-CuS NPs plus PW laser completely ablated cells in the zone of laser exposure (Figure 2). These results showed that PEG-CuS NPs could mediate effective cell killing by photothermolysis, consistent with our earlier reported findings.<sup>33,34</sup>

To investigate whether photothermolysis with CuS NPs and PW laser could sensitize tumors to  $\alpha$ PD-1 immune checkpoint blockade therapy, we analyzed immune cells in B16-OVA tumors treated with combined photothermolysis and  $\alpha$ PD-1 (Figure 3A). Compared to a no-treatment control, combined photothermolysis and  $\alpha$ PD-1 significantly delayed tumor growth, resulting in smaller tumors on day 6 after initiation of laser treatment ( $p < 0.05$ ) (Figure 3B). However, the differences in tumor size between the no-treatment control group and the groups treated with  $\alpha$ PD-1 alone or photothermolysis alone were not statistically significant (Figure 3B). Figure 3C shows the tumor growth curves of individual animals in each treatment group. A significant delay in tumor growth was observed in mice treated with combined photothermolysis and  $\alpha$ PD-1. In comparison, all mice in the untreated control group exhibited rapid tumor growth.

Significantly more CD8<sup>+</sup> ( $p < 0.001$ ) and CD4<sup>+</sup> ( $p < 0.01$ ) T cells were observed in the tumors of mice treated with combined photothermolysis and  $\alpha$ PD-1 than in the tumors of untreated mice, mice treated with photothermolysis alone, or mice treated with  $\alpha$ PD-1 alone (Figure 4A, 4B). In addition, there were significantly more antigen-presenting cells, including CD45<sup>+</sup>CD11b<sup>+</sup>CD169<sup>+</sup> macrophages and CD45<sup>+</sup>CD11b<sup>+</sup>CD11c<sup>+</sup> DCs, in the tumors of mice treated with photothermolysis and  $\alpha$ PD-1 than in the tumors of untreated mice and mice treated with photothermolysis alone or  $\alpha$ PD-1 alone ( $p < 0.05$ ) (Figure 4A, 4C). The absolute numbers of these infiltrated immune cells in the tumors are summarized in Supplementary Figure S4. Increased tumor infiltration of CD11b<sup>+</sup> myeloid cells after photothermolysis was also confirmed by PET/CT imaging with <sup>64</sup>Cu-labeled anti-CD11b antibody (Supplementary Figure S5).

These data suggested that addition of  $\alpha$ PD-1 to photothermolysis may improve tumor antigen presentation and CD8<sup>+</sup> cytotoxic T cell effect on the tumor and supported the idea that anti-immune checkpoint antibody could lessen immunosuppression in the tumor microenvironment and enhance the antitumor effect.

### Combined photothermolysis, PG-CpG, and $\alpha$ PD-1 induced systemic immune response in a poorly immunogenic syngeneic ovarian cancer model

As outlined above, using the B16-OVA melanoma model, we demonstrated that photothermolysis plus  $\alpha$ PD-1 facilitated tumor infiltration of CD8<sup>+</sup> T cells and DCs without increasing populations of immunosuppressive Tregs and MDSCs. However, it remained unclear whether these approaches would be effective in other tumor types. A previous report showed that a derivative of ID8 murine ovarian tumor had 39 transcribed, missense

mutations. An attempt to immunize mice with synthetic peptide vaccines encoding the relevant mutations in this model failed to prolong survival time of tumor-bearing mice.<sup>35</sup> These findings suggest that in tumor types with low mutation burden, vaccination with tumor-specific antigens has limited efficacy. Because tumor infiltration of T cells is positively associated with survival outcome in patients with ovarian cancer,<sup>29,36</sup> increasing recruitment of immune cells to the tumor and tumordraining lymph nodes where DCs are activated to enhance antigen cross-presentation and T cell priming would be highly desirable. Robust activation of immunity requires stimulation of positive costimulatory signals and inhibition of negative immune regulatory signals.

Our preliminary data (Supplementary Figure S6) showed that PG-CpG alone and PG-CpG in combination with photothermolysis displayed only marginal antitumor activity against poorly immunogenic syngeneic ID8-ip1-Luc ovarian tumor. To test whether addition of an immune checkpoint inhibitor ( $\alpha$ PD-1) could sensitize response to PG-CpG-based treatments, we designed experiments in which both an immunostimulatory agent (PG-CpG) and an immune checkpoint inhibitor ( $\alpha$ PD-1) were combined with photothermolysis in the metastatic ID8-ip1-Luc tumor model (Figure 5A and Figure 6A). In these experiments, the laser was focally delivered to the primary subcutaneous ID8-ip1-Luc tumor (Supplementary Figure S7). Because bioluminescent imaging could not be reliably used to estimate tumor burden in mice with intraperitoneal ascites, we used overall survival time as the endpoint. Mice with extensive tumor burden died of accumulation of a large amount of intraperitoneal ascites and/or severe body weight lost (cachexia) (Supplementary Figure S8).

In the first experiment, outlined in Figure 5A, ID8-ip1-Luc tumor-bearing mice were given an intravenous dose of 8 OD/200  $\mu$ l PEG-CuS NPs, and subcutaneous ID8-ip1-Luc tumors were irradiated with PW laser (2.2 W/cm<sup>2</sup>, 1 min) 24 h later. These mice were given a second dose of 8 OD/20  $\mu$ l PEG-CuS NPs intratumorally 1 week later, followed by PW laser irradiation (2.2 W/cm<sup>2</sup>, 1 min) and treatments with PG-CpG and  $\alpha$ PD-1. Then, ID8-ip1-Luc cells were injected again intraperitoneally to mimic metastasis. The results showed no difference in median survival among the mice that received PEG-CuS NPs and PW laser (photothermolysis alone), PG-CpG plus  $\alpha$ PD-1 (immunotherapy alone), and no-treatment (control). However, combination treatment with photothermolysis (PEG-CuS NPs with PW laser) and immunotherapy (PG-CpG and  $\alpha$ PD-1) significantly increased median survival after the intraperitoneal challenge with ID8-ip1-Luc OC cells compared to the no-treatment control, photothermolysis alone, or immunotherapy alone ( $p < 0.01$ , log-rank test) (Figure 5B).

In this study, we used a poorly immunogenic syngeneic ID8-ip1-Luc ovarian cancer mouse model to investigate whether combining PG-CpG and  $\alpha$ PD-1 potentiated photothermolysis of a primary tumor to impede the development of metastatic intraperitoneal tumors. Although the growth of the metastatic intraperitoneal tumors was unaffected by photothermolysis alone directed at the subcutaneous tumor, the combination of photothermolysis and immunotherapy significantly prolonged median survival time of treated mice.

Next, we asked whether photothermal ablation could be optimized to induce durable response. In the second experiment, outlined in Figure 6A, the intravenous dose of PEG-CuS NPs was increased to 20 OD/200  $\mu$ L, and the PW laser exposure time was increased to 2 min. The doses and schedule of PG-CpG and  $\alpha$ PD-1 were kept the same as in the first experiment. In addition, one versus two cycles of photothermal ablation was compared to evaluate possible effects of photothermal ablation on antitumor effects of combination therapy. As expected, the results showed that the median overall survival of mice re-inoculated with ID8-ip1-Luc cells at a distant site (intraperitoneal) was significantly longer in mice treated with combined photothermal ablation (PEG-CuS NPs with PW laser) and immunotherapy (PG-CpG and  $\alpha$ PD-1) than in mice treated with photothermal ablation alone or surgery alone ( $p < 0.0001$ , log-rank test) (Figure 6B). These results demonstrated that photothermal ablation could be optimized to improve the outcome of combination treatment (photothermal ablation and immunotherapy) with regard to PEG-CuS NPs dosing and laser exposure time. However, there was no difference between one and two cycles of photothermal ablation (PEG-CuS NPs with PW laser) in the presence or absence of immunotherapy.

Significantly, only treatments combining photothermal ablation with PG-CpG and  $\alpha$ PD-1 resulted in long-term survival (up to 6 months) in a fraction of mice (Figure 6B). The distribution of body weight of individual mice in all treatment groups was tight initially but varied greatly when the health of mice in the untreated control group and photothermal ablation alone group deteriorated over time (Supplementary Figure S9). These mice performed poorly and became moribund. Their body weight either increased owing to increase in intraperitoneal ascites or decreased owing to loss of appetite and physical activity. On day 94 (~3 months) after the initiation of laser treatments, all mice (8 out of 8) in the untreated group and the group treated with two cycles of photothermal ablation had died, and only 1 of 8 mice remained alive in the group of mice treated with one cycle of photothermal ablation. In comparison, 6 of 10 mice were still alive in the group treated with one cycle of photothermal ablation plus immunotherapy, and 5 of 8 mice were still alive in the group treated with two cycles of photothermal ablation plus immunotherapy.

### **Combined photothermal ablation, PG-CpG, and $\alpha$ PD-1 induced durable response with memory T cells in a poorly immunogenic syngeneic ovarian cancer model**

The immune system can maintain antigen memory for several decades. Therefore, we evaluated immune memory induced by combined photothermal ablation (PEG-CuS NPs with PW laser), PG-CpG, and  $\alpha$ PD-1. From each of the groups treated with one or two cycles of photothermal ablation plus PG-CpG and  $\alpha$ PD-1, we euthanized one mouse that had rejected ID8-ip1-Luc tumor cell challenge and survived for at least 6 months. At gross necropsy, no tumor nodules were found in the peritoneal cavity of these two mice. ELISPOT assay of splenocytes showed 2.7 times as many IFN- $\gamma$ -secreting T cells as did splenocytes from normal control mice (Supplementary Figure S10A). In addition, compared to splenocytes from normal control mice, the splenocytes from the mice that had rejected ID8-ip1-Luc tumor cell challenge had an obvious increasing trend in CD4<sup>+</sup> memory T cells (CD4<sup>+</sup>CD44<sup>hi</sup>CD62L<sup>lo</sup>), CD8<sup>+</sup> memory T cells (CD8<sup>+</sup>CD44<sup>hi</sup>CD62L<sup>lo</sup>), CD4<sup>+</sup> effector T cells (CD4<sup>+</sup>CD44<sup>lo</sup>CD62L<sup>lo</sup>), and CD8<sup>+</sup> effector T cells (CD8<sup>+</sup>CD44<sup>lo</sup>CD62L<sup>lo</sup>) (Supplementary Figure S10B and S10C). Because the naive T cells (CD44<sup>lo</sup>CD62L<sup>hi</sup>) had

been activated and differentiated into memory T cells and effector T cells after they had encountered ID8-ip1-Luc tumor antigen, the percentage of naive T cells decreased (Supplementary Figure S10C).

## Discussion

Findings from this study support the concept that the combination of PW laser-induced, NIR light-absorbing NP-mediated photothermolysis with immunotherapy ( $\alpha$ PD-1 plus PG-CpG) can prolong the survival time of tumor-bearing mice.

One of the unique features of photothermolysis induced by short laser pulses is that it is highly spatially confined.<sup>10</sup> Alternatively, a pulsed laser may be more efficient in generating immunogenic cell death because it can rapidly disrupt the cell membrane and thus may cause rapid release of tumor-associated antigens and danger signals. Further studies are needed to determine how differences in cell death modes caused by laser treatments impact the immunogenicity of dying tumor cells.

Kawakubo et al.<sup>37</sup> recently reported that a combination of  $\alpha$ PD-1 with an ultrafast fractional CO<sub>2</sub> laser (300 Hz) that emits energy at 10,600-nm infrared radiation showed antitumor immunity in a subcutaneous CT26 colon cancer model. We note several differences between the Nd:YAG laser (PW laser) used in the current study and the CO<sub>2</sub> laser used in the earlier study. First, the Nd:YAG laser emits energy at 1064 nm, which allows deeper tissue penetration than the 10,600-nm laser because water absorption coefficients for the 1064-nm and 10,600-nm laser beams were 0.1 cm<sup>-1</sup> and 10<sup>3</sup> cm<sup>-1</sup>, respectively. The CO<sub>2</sub> laser is applicable only for the treatment of superficial tissues. Second, the Nd:YAG laser can provide high-power (~ megawatts) pulsed radiation using Q-switched technology, and therefore it is possible to achieve a high-fluence rate at large beam size. In contrast, the fractional CO<sub>2</sub> laser has limited radiation power (<100 watts). Consequently, its beam has to be spatially focused to a small size (~0.5 mm) to obtain sufficient power density. Lastly, with the Nd:YAG laser, because of reduced interference from water, it is possible to introduce exogenous light-absorbing agents (e.g., PEG-CuS NPs) to ablate tumor tissues with high selectivity.

In two independent experiments with the poorly immunogenic ID8-ip1-Luc ovarian cancer model, photothermolysis alone did not show an antitumor effect in terms of tumor growth delay or mouse survival, whether one or two cycles of photothermolysis were given. However, the median survival time of mice re-inoculated with ID8-ip1-Luc tumor cells at a distant site (peritoneum) was significantly prolonged when photothermolysis was combined with immunotherapy (PG-CpG +  $\alpha$ PD-1). These results imply that without the help of immunostimulatory agents, enhanced exposure of tumor-specific antigens by photothermolysis could be negated by immune suppression mechanisms present in the tumor microenvironment.

It is well known that immune checkpoint pathways are a major mechanism of immune evasion in tumors. Checkpoint inhibitory molecules such as  $\alpha$ PD-1 and anti-PD-L1 antibody have increasingly been considered as new strategies for cancer immunotherapy because of

their demonstrated activity in multiple types of cancers. A notable finding of our study was that a fraction of mice challenged with ID8-ip1-Luc cells at a distant site displayed durable response when photothermolysis induced by CuS NPs plus PW laser was combined with PG-CpG and  $\alpha$ PD-1 immunotherapy, while treatment with photothermolysis or immunotherapy alone did not show such an effect. ELISPOT assay confirmed that splenocytes from the long-term-surviving mice had more IFN- $\gamma$ -secreting T cells than splenocytes from the normal control mice had. Memory T cells, which reside in both lymphoid and nonlymphoid tissues, can elicit immediate protection by producing cytokines such as IFN- $\gamma$ , which is one of the key markers of cellular immunity in antitumor immunotherapy. Further analysis showed increase in memory and effector T cell populations in the splenocytes of the long-term-surviving mice compared to the normal control mice. These results indicated that these long-term-surviving mice successfully established antitumor immunity. Further studies are warranted to elucidate the mechanisms of immunogenic cell death induced by PW laser, to determine optimal treatment conditions that further increase the percentage of mice with durable response, and to develop cost-effective tools for convenient delivery of PW laser beam to diseased sites in the surgical suite. Such advances will ultimately facilitate translation of this new treatment modality into the clinic.

In summary, photothermolysis based on NIR light-absorbing CuS NPs and short pulses from a PW laser is a promising interventional technique that may synergize with Toll-like receptor agonists and immune checkpoint inhibitors to enhance the abscopal effect on tumors and prolong mouse survival.

## Supplementary Material

Refer to Web version on PubMed Central for supplementary material.

## Acknowledgments

Financial support:

The authors thank Ms. Stephanie P. Deming of Scientific Publications, Research Medical Library, MD Anderson Cancer Center, for editing the manuscript. We acknowledge that this work was supported in part by the John S. Dunn, Sr., Distinguished Chair in Diagnostic Imaging (Dr. William A. Murphy, Jr.) and by the University Cancer Foundation via the Institutional Research Grant program at The University of Texas MD Anderson Cancer Center. Additionally, A.K.S. was supported by grants P50 CA217685 and R35 CA209904 from the National Cancer Institute; the American Cancer Society Research Professor Award; and the Frank McGraw Memorial Chair in Cancer Research. We acknowledge support by the NIH/NCI under award number P30CA016672 for the use of the High-Resolution Electron Microscopy, Flow Cytometry & Cellular Imaging, and Small Animal Imaging core facilities.

## List of abbreviations

<b>PW laser</b>	pulsed-wave laser
<b>CuS NPs</b>	copper sulfide nanoparticles
<b>PG-CpG</b>	polymeric conjugate of CpG
<b><math>\alpha</math>PD-1</b>	anti-PD-1 antibody
<b>DCs</b>	dendritic cells

<b>MDSCs</b>	myeloid-derived suppressor cells
<b>i.p.</b>	intraperitoneal
<b>i.t.</b>	intratumoral
<b>i.v.</b>	intravenous
<b>s.c.</b>	subcutaneous
<b>NIR</b>	near-infra red
<b>OD</b>	optical density
<b>IFN-<math>\gamma</math></b>	interferon- $\gamma$

## References

1. Zhou M, Zhang R, Huang M, Lu W, Song S, Melancon MP, et al., A chelator-free multifunctional [64Cu]CuS nanoparticle platform for simultaneous micro-PET/CT imaging and photothermal ablation therapy. *J Am Chem Soc.* 2010;132:15351–8 [PubMed: 20942456]
2. Li Y, Lu W, Huang Q, Huang M, Li C and Chen W, Copper sulfide nanoparticles for photothermal ablation of tumor cells. *Nanomedicine (Lond).* 2010;5:1161–71 [PubMed: 21039194]
3. Zhou M, Tian M and Li C, Copper-based nanomaterials for cancer imaging and therapy. *Bioconjug Chem.* 2016;27:1188–99 [PubMed: 27094828]
4. Zhou M, Ku G, Pigeon L and Li C, Theranostic probe for simultaneous in vivo photoacoustic imaging and confined photothermolysis by pulsed laser at 1064 nm in 4T1 breast cancer model. *Nanoscale.* 2014;6:15228–15235 [PubMed: 25379880]
5. Glazer ES and Curley SA, The ongoing history of thermal therapy for cancer. *Surg Oncol Clin N Am.* 2011;20:229–235 [PubMed: 21377580]
6. Li J, Gupta S and Li C, Research perspectives: gold nanoparticles in cancer theranostics. *Quant Imaging Med Surg.* 2013;3:284–91 [PubMed: 24404441]
7. Mehta A, Oklu R and Sheth RA, Thermal ablative therapies and immune checkpoint modulation: can locoregional approaches effect a systemic response? *Gastroenterol Res Pract.* 2016;2016:9251375 [PubMed: 27051417]
8. Lapotko D, Pulsed photothermal heating of the media during bubble generation around gold nanoparticles. *Int J Heat Mass Tran.* 2009;52:1540–1543
9. Peeters S, Kitz M, Preisser S, Wetterwald A, Rothen-Rutishauser B, Thalmann GN, et al., Mechanisms of nanoparticle-mediated photomechanical cell damage. *Biomed Opt Express.* 2012;3:435–446 [PubMed: 22435092]
10. Ku G, Huang Q, Wen X, Ye J, Piwnica-Worms D and Li C, Spatial and temporal confined photothermolysis of cancer cells mediated by hollow gold nanospheres targeted to epidermal growth factor receptors. *ACS Omega.* 2018;3:5888–5895 [PubMed: 29876540]
11. Assuncao E and Williams S, Comparison of continuous wave and pulsed wave laser welding effects. *Opt Laser Eng.* 2013;51:674–680
12. Demaria S, Ng B, Devitt ML, Babb JS, Kawashima N, Liebes L, et al., Ionizing radiation inhibition of distant untreated tumors (abscopal effect) is immune mediated. *Int J Radiat Oncol.* 2004;58:862–870
13. Twyman-Saint Victor C, Rech AJ, Maity A, Rengan R, Pauken KE, Stelekati E, et al., Radiation and dual checkpoint blockade activate non-redundant immune mechanisms in cancer. *Nature.* 2015;520:373–377 [PubMed: 25754329]
14. Rodriguez-Ruiz ME, Rodriguez I, Garasa S, Barbes B, Solorzano JL, Perez-Gracia JL, et al., Abscopal effects of radiotherapy are enhanced by combined immunostimulatory mabs and are dependent on cd8 t cells and crosspriming. *Cancer Res.* 2016;76:5994–6005 [PubMed: 27550452]

15. Zhang B, Bowerman NA, Salama JK, Schmidt H, Spiotto MT, Schietinger A, et al., Induced sensitization of tumor stroma leads to eradication of established cancer by T cells. *J Exp Med.* 2007;204:49–55 [PubMed: 17210731]
16. Fend L, Yamazaki T, Remy C, Fahrner C, Gantzer M, Nourtier V, et al., Immune checkpoint blockade, immunogenic chemotherapy or ifn-alpha blockade boost the local and abscopal effects of oncolytic virotherapy. *Cancer Res.* 2017;77:4146–4157 [PubMed: 28536278]
17. Chen Q, Xu LG, Liang C, Wang C, Peng R and Liu Z, Photothermal therapy with immune-adjuvant nanoparticles together with checkpoint blockade for effective cancer immunotherapy. *Nat Commun.* 2016;7
18. Waitz R, Solomon SB, Petre EN, Trumble AE, Fasso M, Norton L, et al., Potent induction of tumor immunity by combining tumor cryoablation with anti-ctla-4 therapy. *Cancer Res.* 2012;72:430–439 [PubMed: 22108823]
19. Brix N, Tiefenthaler A, Anders H, Belka C and Lauber K, Abscopal, immunological effects of radiotherapy: narrowing the gap between clinical and preclinical experiences. *Immunol Rev.* 2017;280:249–279 [PubMed: 29027221]
20. Chu KF and Dupuy DE, Thermal ablation of tumours: biological mechanisms and advances in therapy. *Nat Rev Cancer.* 2014;14:199–208 [PubMed: 24561446]
21. Vollmer J, Progress in drug development of immunostimulatory CpG oligodeoxynucleotide ligands for TLR9. *Expert Opin Biol Ther.* 2005;5:673–82 [PubMed: 15934842]
22. Degli-Esposti MA and Smyth MJ, Close encounters of different kinds: dendritic cells and NK cells take centre stage. *Nat Rev Immunol.* 2005;5:112–24 [PubMed: 15688039]
23. Ma Q, Zhou DP, DeLyria ES, Wen XX, Lu W, Thapa P, et al., Synthetic poly(L-glutamic acid)-conjugated CpG exhibits antitumor efficacy with increased retention in tumor and draining lymph nodes after intratumoral injection in a mouse model of melanoma. *J Immunother.* 2017;40:11–20 [PubMed: 27681378]
24. Chen LP and Flies DB, Molecular mechanisms of T cell co-stimulation and co-inhibition. *Nat Rev Immunol.* 2013;13:227–242 [PubMed: 23470321]
25. Hamanishi J, Mandai M and Konishi I, Immune checkpoint inhibition in ovarian cancer. *Int Immunol.* 2016;28:339–48 [PubMed: 27055470]
26. Brahmer JR, Tykodi SS, Chow LQM, Hwu WJ, Topalian SL, Hwu P, et al., Safety and Activity of Anti-PD-L1 Antibody in Patients with Advanced Cancer. *N Engl J Med.* 2012;366:2455–2465 [PubMed: 22658128]
27. Allison JP, Immune checkpoint blockade in cancer therapy: the 2015 Lasker-DeBakey clinical medical research award. *JAMA.* 2015;314:1113–4 [PubMed: 26348357]
28. van Rooij N, van Buuren MM, Philips D, Velds A, Toebes M, Heemskerk B, et al., Tumor exome analysis reveals neoantigen-specific T-cell reactivity in an ipilimumab-responsive melanoma. *J Clin Oncol.* 2013;31:E439–E442 [PubMed: 24043743]
29. Strickland KC, Howitt BE, Shukla SA, Rodig S, Ritterhouse LL, Liu JF, et al., Association and prognostic significance of BRCA1/2-mutation status with neoantigen load, number of tumor-infiltrating lymphocytes and expression of PD-1/PD-L1 in high grade serous ovarian cancer. *Oncotarget.* 2016;7:13587–13598 [PubMed: 26871470]
30. Cao Q, Huang Q, Mohan C and Li C, Small-Animal PET/CT Imaging of Local and Systemic Immune Response Using (64)Cu-alphaCD11b. *J Nucl Med.* 2019;60:1317–1324 [PubMed: 30796172]
31. Lutz MB, Kukutsch N, Ogilvie ALJ, Rossner S, Koch F, Romani N, et al., An advanced culture method for generating large quantities of highly pure dendritic cells from mouse bone marrow. *J Immunol Methods.* 1999;223:77–92 [PubMed: 10037236]
32. Shi S, Wen X, Li T, Wen X, Cao Q, Liu X, et al., Thermosensitive biodegradable copper sulfide nanoparticles for real-time multispectral optoacoustic tomography. *ACS Applied Bio Materials.* 2019;2:3203–3211
33. Zhou M, Melancon M, Stafford RJ, Li J, Nick AM, Tian M, et al., Precision nanomedicine using dual PET and MR temperature imaging-guided photothermal therapy. *J Nucl Med.* 2016;57:1778–1783 [PubMed: 27283932]

34. Zhou M, Li J, Liang S, Sood AK, Liang D and Li C, CuS nanodots with ultrahigh efficient renal clearance for positron emission tomography imaging and image-guided photothermal therapy. *ACS Nano*. 2015;9:7085–96 [PubMed: 26098195]
35. Martin SD, Brown SD, Wick DA, Nielsen JS, Kroeger DR, Twumasi-Boateng K, et al., Low mutation burden in ovarian cancer may limit the utility of neoantigen-targeted vaccines. *PLoS One*. 2016;11:e0155189 [PubMed: 27192170]
36. Scarlett UK and Conejo-Garcia JR, Modulating the tumor immune microenvironment as an ovarian cancer treatment strategy. *Expert Rev Obstet Gynecol*. 2012;7:413–419 [PubMed: 24039628]
37. Kawakubo M, Cunningham TJ, Demehri S and Manstein D, Fractional laser releases tumor-associated antigens in poorly immunogenic tumor and induces systemic immunity. *Sci Rep*. 2017;7:12751 [PubMed: 28986576]

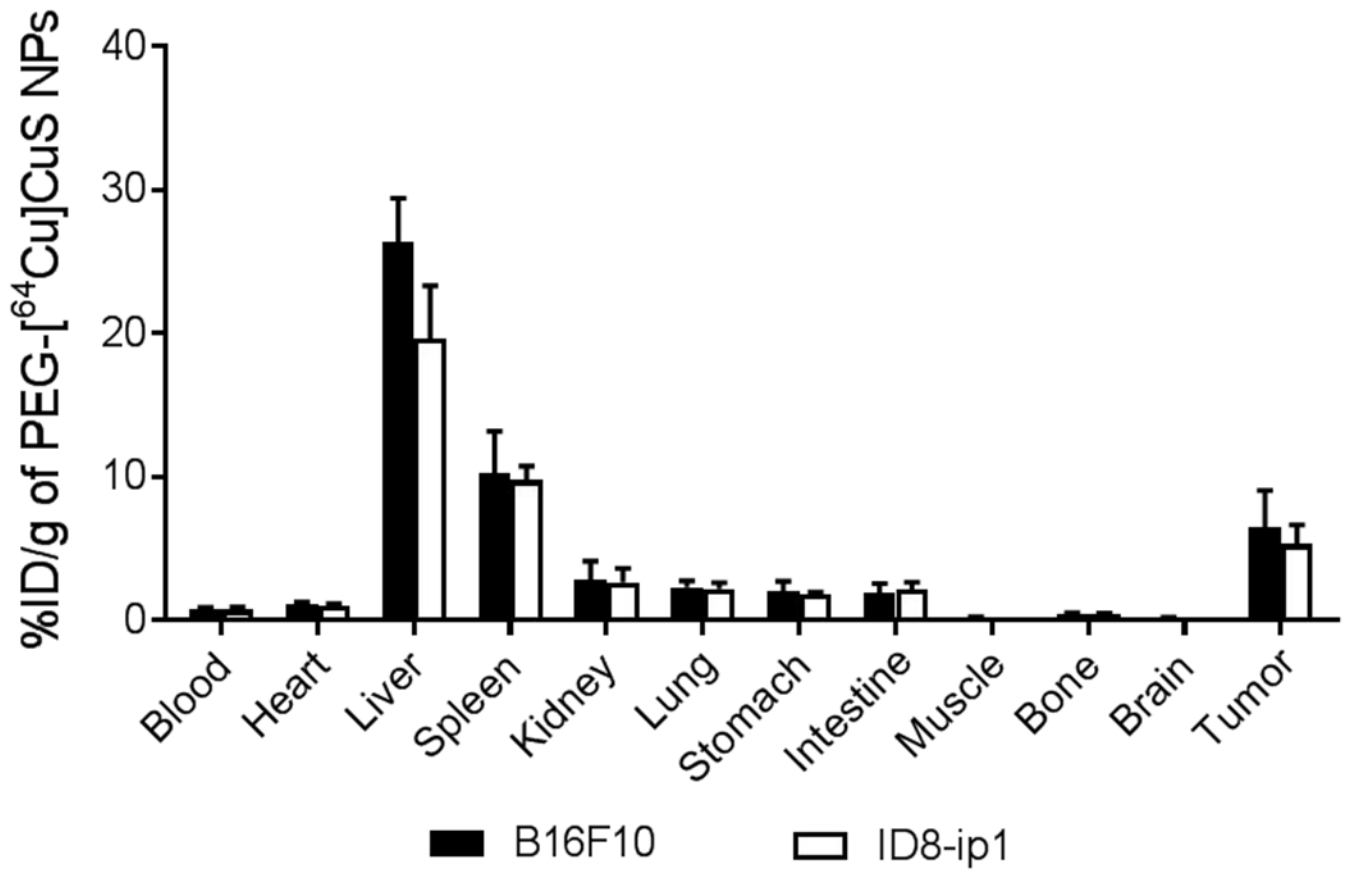


**Figure 1.** Biodistribution of PEG-[<sup>64</sup>Cu]CuS NPs in mice with B16F10 and mice with ID8-ip1-Luc tumors 24 h after injection. Data are presented as the mean  $\pm$  standard deviation (n = 5/group).

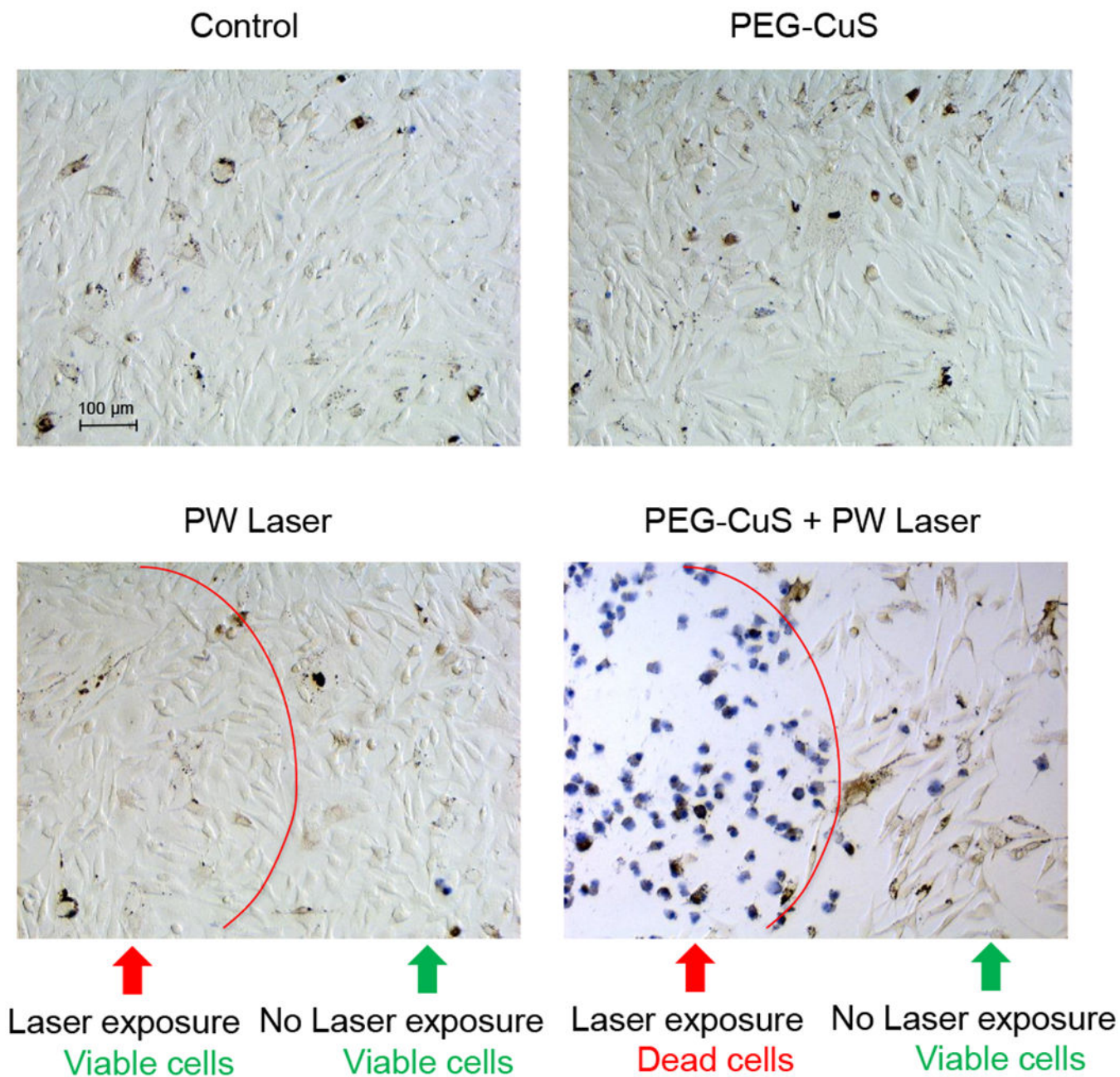


**Figure 2.**

Impact of photothermolysis with PEG-CuS NPs and PW laser on B16-OVA melanoma cells *in vitro*. Cells were incubated with PEG-CuS NPs (2 OD) at 37°C for 2 h. After washing steps, cells were irradiated with 1064-nm PW laser at a power density of 2.2 W/cm<sup>2</sup> for 2 min. Cell viability was visualized by trypan blue staining.

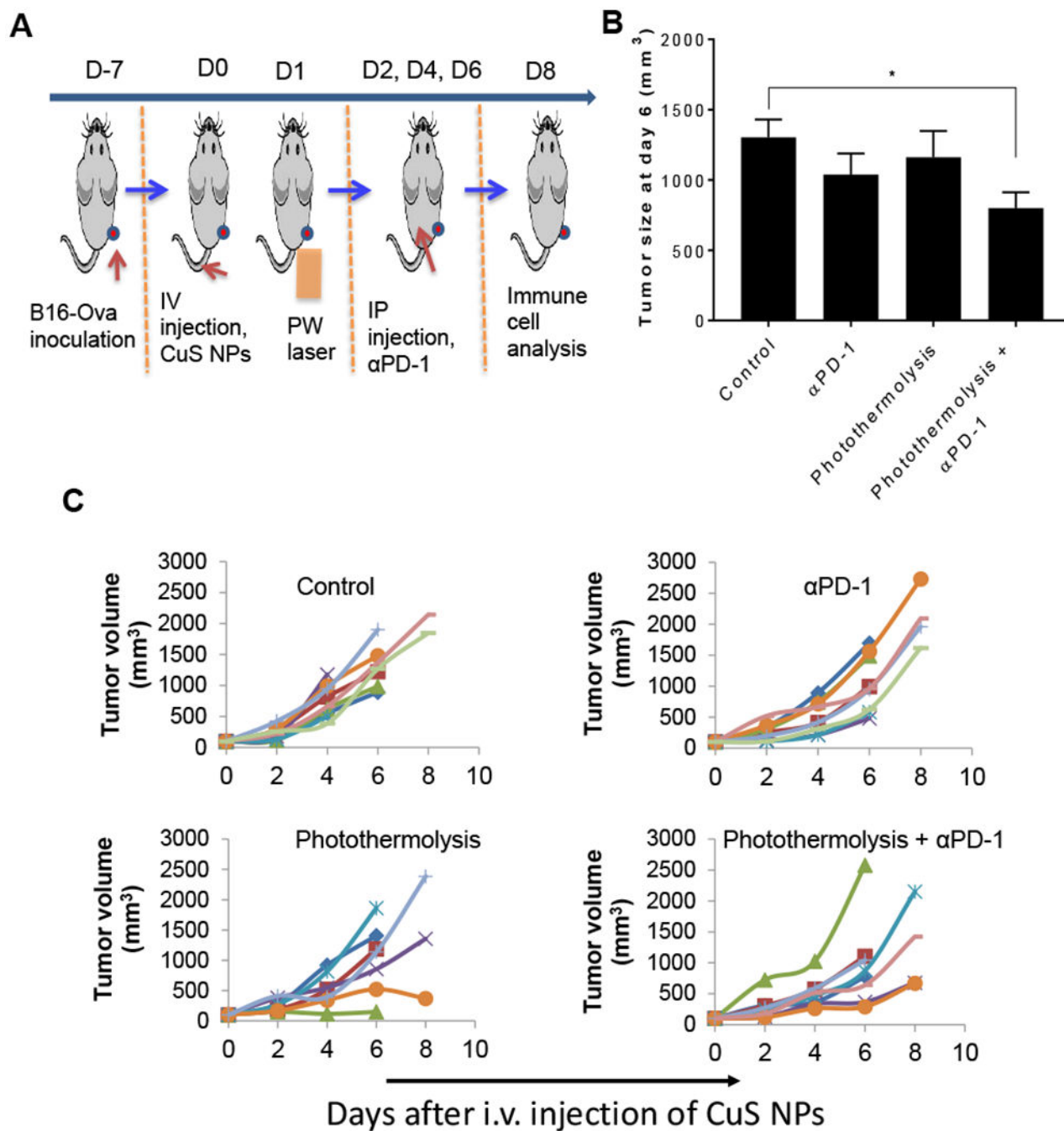


**Figure 3.** Antitumor effect of photothermolysis plus  $\alpha$ PD-1 on B16-OVA tumor-bearing mice. (A) Experimental design diagram. (B) Tumor size at day 6 after laser treatment. Data are presented as the mean  $\pm$  standard error of the mean ( $n = 6$ /group,  $*p < 0.05$ ). (C) B16-OVA tumor growth curves in individual animals in groups of untreated control mice and mice treated with  $\alpha$ PD-1 alone, photothermolysis alone (PEG-CuS NPs + PW laser), and combined photothermolysis +  $\alpha$ PD-1. In each panel, each line represents one mouse.

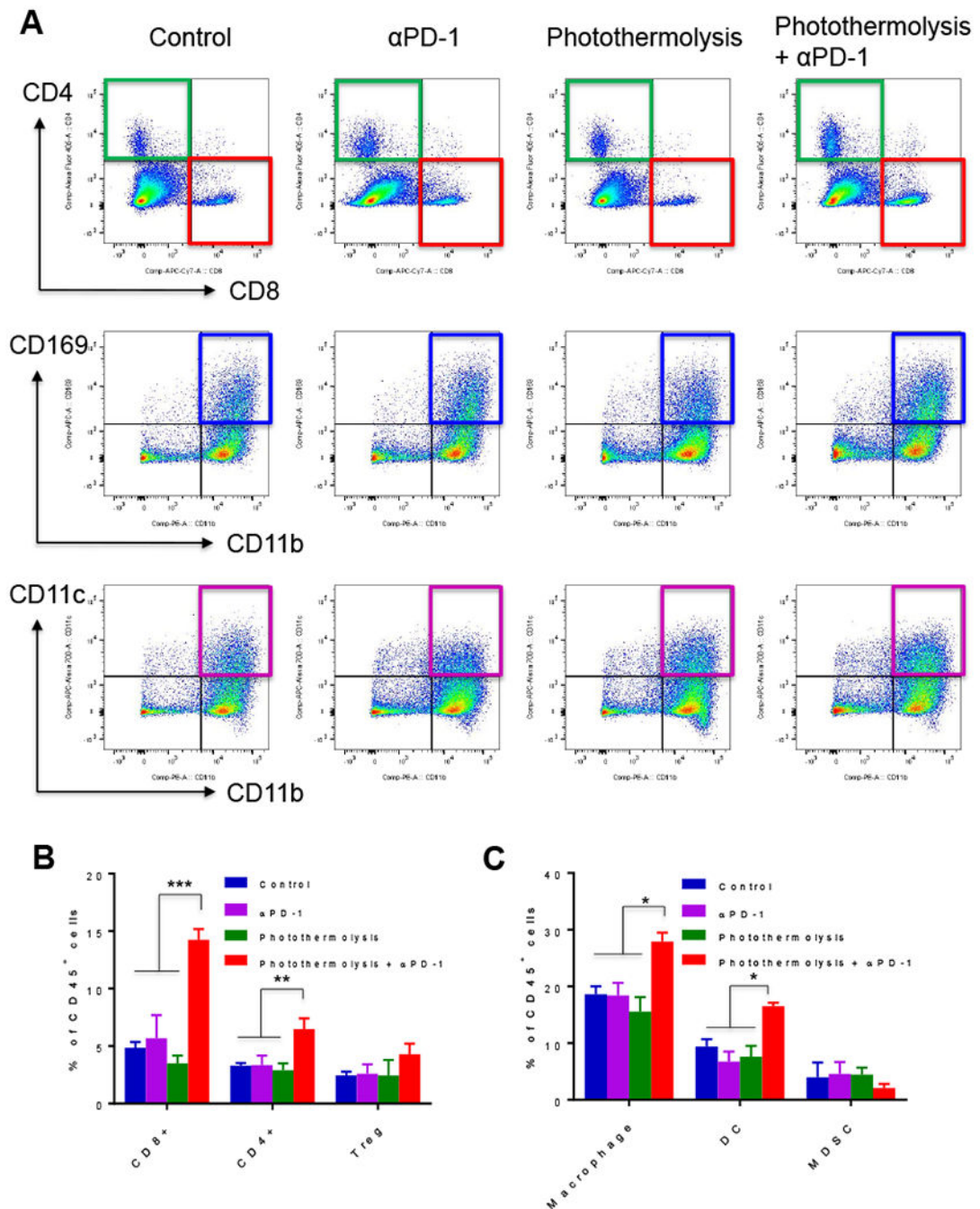


**Figure 4.** Effect of photothermolysis mediated by CuS NPs plus PW laser in combination with αPD-1 on tumor infiltration of T cells, antigen-presenting cells, and myeloid cells in B16-OVA tumor. (A) Representative flow cytometry images. (B, C) Analysis of tumor infiltration of (B) T cells and (C) macrophages (CD45<sup>+</sup>CD11b<sup>+</sup>CD169<sup>+</sup>), DCs (CD45<sup>+</sup>CD11b<sup>+</sup>CD11c<sup>+</sup>), and MDSCs (CD45<sup>+</sup>CD11b<sup>+</sup>Gr1<sup>+</sup>). Data are presented as the mean ± standard error of the mean (n = 3). \*p<0.05, \*\*p<0.01, \*\*\*p<0.001.

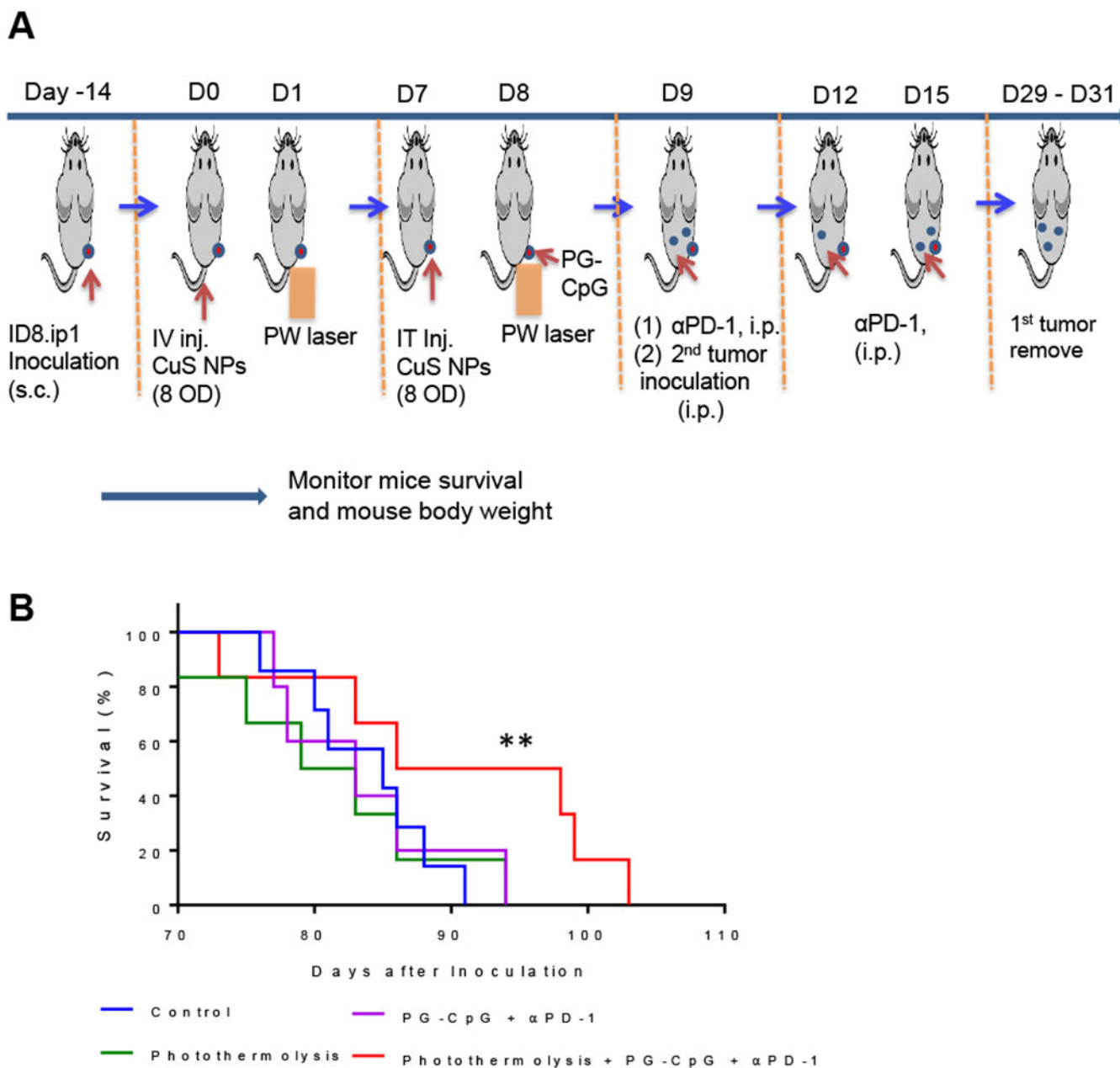


**Figure 5.** Survival of mice re-inoculated with ID8-ip1-Luc ovarian cancer cells after combined photothermolysis and immunotherapy. (A) Experimental design diagram. (B) Kaplan-Meier survival curves. Combination treatment (8 OD CuS NPs + PW laser 1 min + PG-CpG + αPD-1 groups) compared to photothermolysis alone, immunotherapy alone, and untreated control group (n = 10/group). \*\*p<0.01, log-rank Mantel-Cox test. i.p., intraperitoneal; i.t., intratumoral; i.v., intravenous; s.c., subcutaneous.

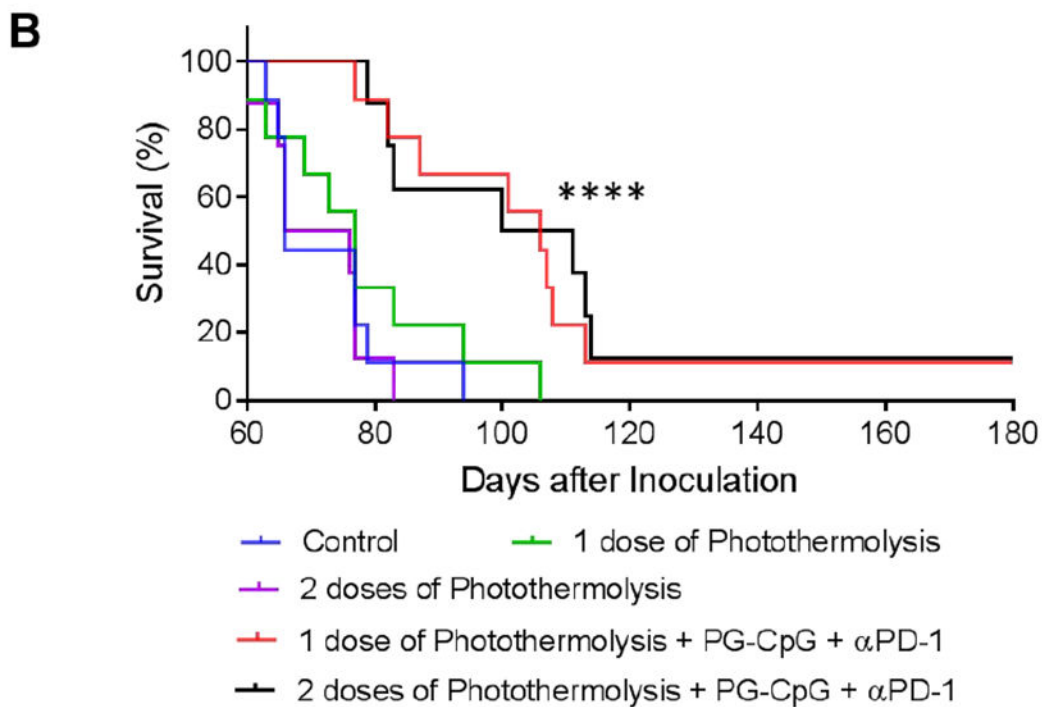
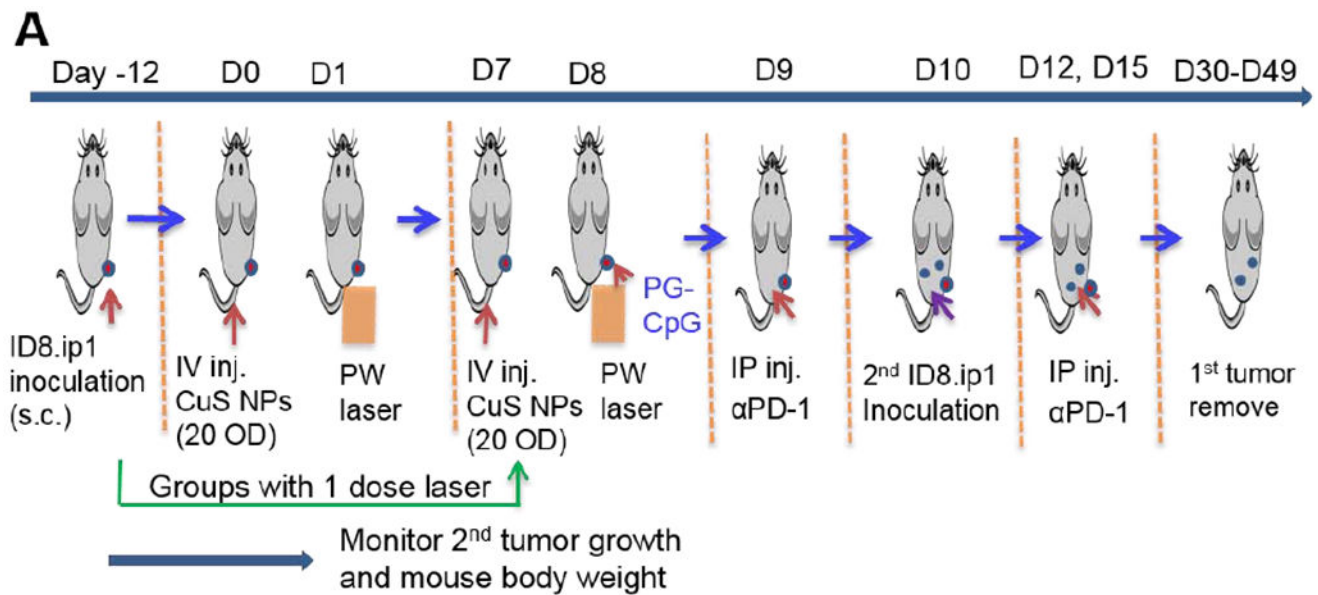


**Figure 6.**

Survival of mice re-inoculated with ID8-ip1-Luc ovarian cancer cells after combined photothermolysis and immunotherapy, with one or two rounds of photothermolysis. (A) Experimental design diagram. (B) Kaplan-Meier survival curves for mice monitored for up to 182 days after institution of laser treatment. \*\*\*\* $p < 0.0001$  for combination treatment (20 OD CuS NPs + PW laser 2 min + PG-CpG + αPD-1 groups) compared to photothermolysis alone and untreated control group (log-rank Mantel-Cox test;  $n = 9$  for the control, one round of photothermolysis, and one round of photothermolysis + PG-CpG + αPD-1 groups);

n = 8 for the two rounds of photothermolysis and two rounds of photothermolysis + PG-CpG +  $\alpha$ PD-1 groups), i.p., intraperitoneal; i.v., intravenous; s.c., subcutaneous.

Author Manuscript

Author Manuscript

Author Manuscript

Author Manuscript